Resonant modes of a bottle-shaped cavity and their effects in the response of finite and infinite gratings

Ricardo A. Depine* and Diana C. Skigin†
Grupo de Electromagnetismo Aplicado, Departamento de Física, Facultad de Ciencias Exactas y Naturales, Universidad de Buenos Aires, Ciudad Universitaria, Pabellón I, 1428 Buenos Aires, Argentina
(Received 28 September 1999)

The resonant frequencies of a one-dimensional bottle-shaped cavity embedded in a ground plane are calculated using a modal approach for *s* and *p* polarizations. The same formalism is used to solve the problem of scattering from a surface with a finite number of cavities and from an infinite periodic grating. We show numerical results where the resonant behavior is evidenced as dips in the curve of intensity specularly reflected from a surface with one or several bottle-shaped grooves. The surface shape resonances of a single cavity are also shown to have a great influence on the efficiency distribution of the diffracted orders from infinite gratings made of bottle-shaped cavities. The excitation of even and odd modes is analyzed for both polarizations.

PACS number(s): 42.25.Fx, 42.25.Bs

I. INTRODUCTION

The excitation of surface shape resonances and its relation with intensification phenomena such as backscattering enhancement have attracted many studies in recent years. In addition, it is known that an interface between air and a perfect conductor can support *p*- (and not *s*-) polarized surface waves. It was found that these waves can be excited by adding roughness to the surface [1]. However, the resonant behavior of infinitely periodic gratings of lamellar profile has also been studied by many authors, in particular for *s* polarization [2–4]. Numerical evidence of a close relationship between *s* resonances and the excitation of *s*-polarized surface waves was given [5].

The resonant features of an isolated cavity or groove have also been investigated by means of different implementations of two basic approaches: integral and modal methods [6–9]. The results show that for an *s*-polarized electromagnetic field, a strong intensification inside the cavity is found for certain wavelengths when its profile is described by a bivalued function of the coordinates, such as a slotted cylinder or a bottle-shaped groove [8,9]. This suggests that it might be possible to excite *s*-polarized surface waves in metallic structures with bivalued cavities, and this constitutes one of the motivations of the present paper.

The modal formalism, employed here to solve the homogeneous problem, the scattering problem from a plane surface with several cavities, and the diffraction problem from an infinite grating, was first formulated to deal with simple geometries of the grooves such as rectangular [3], triangular [10], or semicircular [11]. Later it was generalized for arbitrary shapes of the grooves [12,13]. In the present paper, we take advantage of the rectangular geometry of the bottle-shaped cavity and the implementation of the modal method results in a simple and efficient way to calculate the fields, without the need of any sophisticated algorithm. In addition, this particular shape allows us to vary independently the geometrical parameters (widths and depths) to analyze the dependence of the resonant phenomenon with each one.

The purpose of the present paper is to study the resonant characteristics of a bottle-shaped cavity, and the effects that these resonances produce in the scattering pattern from finite and infinite gratings. A deep understanding of this phenomenon might provide us with a key to explore the existence of *s*-polarized surface waves in metallic surfaces with bivalued corrugations.

The paper is organized as follows. In Sec. II we solve the homogeneous problem of a cavity in a ground plane, and find resonant wavelengths of the groove for both modes of polarization using a modal approach. The same formalism is used to solve the scattering problem of a Gaussian beam impinging on a surface with a finite number of grooves, as well as the diffraction problem of a plane wave on an infinite grating. In Sec. III we first give numerical results that validate the procedure followed to find the resonant depths of a cavity. Then some interesting examples are shown for *s* and *p* polarizations. Curves of specularly reflected intensity and diffracted efficiency as a function of the depth are also shown, where the resonant behavior of the cavity is strongly marked. The final comments and conclusions are given in Sec. IV.

II. EIGENMODES OF A SINGLE CAVITY

To find resonant wavelengths associated with the geometrical characteristics of a single cavity, we solve the homogeneous problem for a bottle-shaped cavity of widths c_1 and c_2 and heights h_1 and h_2 (see Fig. 1) on a ground plane. The groove is along the $\hat{z}$ direction, and due to the symmetry of the problem it can be separated into basic modes of polarization *s* (electric field parallel to the groove) and *p* (magnetic field parallel to the groove). Each polarization case allows a scalar treatment.

We divide the space into three regions: region 1 (inside the cavity), region 2 (the neck of the cavity), and region 3 (the upper half-space, as shown in Fig. 1). In what follows we unify the notation and denote $E_z(x,y)$ by $f^s(x,y)$ in the *s* case and $H_z(x,y)$ by $f^p(x,y)$ in the *p* case. In regions 1 and 2 (the subscript $j=1$ and 2 denotes the region), the fields are

*Electronic address: rdep@df.uba.ar
†Electronic address: dcs@df.uba.ar

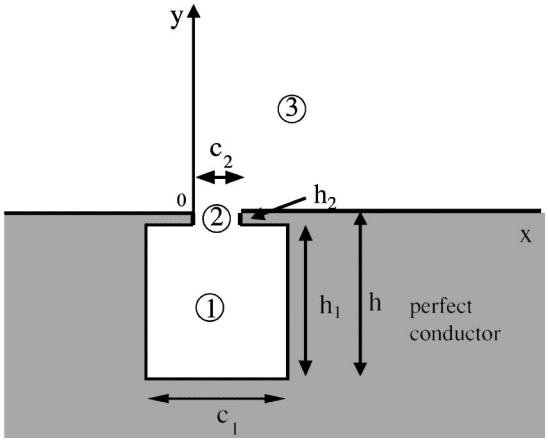

FIG. 1. The structure under study: a bottle-shaped groove along the z direction, on a ground plane. The cavity has total depth $h=h_1+h_2$, and the maximum and minimum widths are c_1 and c_2.

expanded in their modal eigenfunctions:

$$f_j^q(x,y)=\sum_{m=0}^{\infty} u_{jm}^q(x)w_{jm}^q(y), \quad j=1,2 \tag{1}$$

where

$$u_{1m}^q(x)=\begin{cases}\sin\left[\dfrac{m\pi}{c_1}(x-x_1)\right] & \text{for } q=s\\ \cos\left[\dfrac{m\pi}{c_1}(x-x_1)\right] & \text{for } q=p,\end{cases} \tag{2}$$

$$w_{1m}^q(y)=\begin{cases}A_m^s\sin[\mu_{m1}(y+h)] & \text{for } q=s\\ A_m^p\cos[\mu_{m1}(y+h)] & \text{for } q=p,\end{cases} \tag{3}$$

$$u_{2m}^q(x)=\begin{cases}\sin\left[\dfrac{m\pi x}{c_2}\right] & \text{for } q=s\\ \cos\left[\dfrac{m\pi x}{c_2}\right] & \text{for } q=p,\end{cases} \tag{4}$$

$$w_{2m}^q(y)=[a_m^q\sin(\mu_{m2}y)+b_m^q\cos(\mu_{m2}y)], \quad q=s,p, \tag{5}$$

$$\mu_{mj}=\begin{cases}\sqrt{k^2-\left[\dfrac{m\pi}{c_j}\right]^2} & \text{if } k^2>\left[\dfrac{m\pi}{c_j}\right]^2\\ i\sqrt{\left[\dfrac{m\pi}{c_j}\right]^2-k^2} & \text{if } k^2<\left[\dfrac{m\pi}{c_j}\right]^2.\end{cases} \tag{6}$$

$k=|\vec{k}|=\omega/c$, and A_m^q, a_m^q, and b_m^q are unknown complex amplitudes. Notice that $u_{j0}^s(x)=0$, and then the sum in Eq. (1) starts from $m=1$ in the s case. The functions $u_{1m}^q(x)$ satisfy the appropriate boundary conditions at $x=x_1$ and at $x=x_1+c_1$, the functions $u_{2m}^q(x)$ satisfy the boundary conditions at $x=0$ and at $x=c_2$, and the functions $w_{1m}^q(y)$ satisfy the boundary condition at $y=-h$, according to the case of polarization. Since we are interested in finding the surface shape resonances, the total field in region 3 is an outgoing field, and can be represented by a continuum of outgoing plane waves,

$$f_3^q(x,y)=\int_{-\infty}^{\infty}\mathcal{R}^q(\alpha)e^{i(\alpha x+\beta y)}d\alpha, \tag{7}$$

where

$$\beta=\begin{cases}\sqrt{k^2-\alpha^2} & \text{if } k^2>\alpha^2\\ i\sqrt{\alpha^2-k^2} & \text{if } k^2<\alpha^2,\end{cases} \tag{8}$$

and $\mathcal{R}^q(\alpha)$ is an unknown function.

To solve the problem, the fields in regions 1 and 2 are matched at the interface $y=-h_2$ and the fields in regions 2 and 3 are matched at $y=0$. This generates four x-dependent equations for each polarization, that are projected in convenient bases (for the explicit form of these equations, see Appendix A). Then, after several substitutions, we obtain a homogeneous matrix equation for the vector of modal amplitudes A^q $(q=s,p)$:

$$\mathbf{M}^qA^q=\mathbf{0}, \quad q=s,p. \tag{9}$$

The explicit expressions of the matrix elements are given in Appendix B. The final equation can be obtained in many different ways. For instance, we could have derived a matrix equation for the amplitudes in the neck of the groove a_m^q or b_m^q. However, since we are interested in finding the wavelengths at which the field within the widest part of the cavity is enhanced, it is convenient to express all the unknowns in terms of the modal amplitudes in region 1, to obtain Eq. (9). Then the resonant wavelengths of the groove (λ_{res}) are those at which the determinant of the matrix $\mathbf{M}^q$ vanishes. Or, conversely, for a fixed wavelength the resonant depths h_1 are those at which the determinant vanishes. The solutions of $\det[\mathbf{M}^q]=0$ are complex: the real part is associated with the resonant parameter (wavelength, depth), whereas the imaginary part is related to the quality of the resonance. To find the resonant values we have numerically evaluated the function $|\det[\mathbf{M}^q]|^{-2}$, and, then, plotting this function against the corresponding variable, we find peaks centered at the real parts of the resonant values [14,15,7].

III. SCATTERING PROBLEM

The resonant effects occuring in a single cavity are expected to show up somehow in the scattering pattern of a surface with one or more identical grooves. Then we solved the scattering problem of a surface with a finite number of bottle-shaped grooves illuminated by a limited beam, and also the diffraction problem of a plane wave incident upon an infinite grating. These situations are considered in Secs. III A and III B.

A. Finite grating

The scattering problem from a perfectly conducting surface with N localized bottle-shaped cavities is solved by the modal approach [9]. We consider the general case where the widths c_1 and c_2 and the depths h_1 and h_2 of each cavity can vary. The procedure to find the solution is essentially the same as that used for the homogeneous problem, but in this case it is necessary to find the field expansions in each one of the cavities. Then the fields in regions 1 and 2 are written as

$$f_j^q(x,y)=\sum_{m=0}^{\infty} u_{jm}^{ql}(x)w_{jm}^{ql}(y)\mathrm{rect}\left(\frac{x-x_j^l}{c_j^l}\right), \quad j=1,2 \tag{10}$$

where the explicit expressions of the functions $u_{jm}^{ql}(x)$ and $w_{jm}^{ql}(y)$ are given in Appendix C. In region 3, the total field is the sum of the incident field—a limited Gaussian beam—and the scattered field given by Eq. (7):

$$f_3^q(x,y)=\int_{-k}^{k}\mathcal{A}(\alpha)e^{i(\alpha x-\beta y)}d\alpha+\int_{-\infty}^{\infty}\mathcal{R}^q(\alpha)e^{i(\alpha x+\beta y)}d\alpha, \tag{11}$$

where

$$\mathcal{A}(\alpha)=\frac{w}{2\sqrt{\pi}}\exp\left\{-(\alpha-\alpha_0)^2\left(\frac{w}{2}\right)^2\right\}\exp[i(\alpha-\alpha_0)b], \tag{12}$$

$$b=\frac{\beta_0}{k}x_0. \tag{13}$$

w is the spatial width of the beam, x_0 is the x coordinate on the surface where the center of the beam impinges upon the structure, β is defined in Eq. (8), $\alpha_0=k\sin\theta_0$, $\beta_0=k\cos\theta_0$, and θ_0 is the angle of incidence measured from the normal to the mean surface.

We discretize and truncate the integrals in Eq. (11), and proceed as in Sec. II to obtain, in this case, an inhomogeneous matrix equation. However, since we are now interested in calculating the scattered intensity which is proportional to $|\mathcal{R}^q(\alpha_n)|^2$, it is more convenient to derive a matrix equation for the unknown Rayleigh amplitudes $\mathcal{R}^q(\alpha_n)=\mathcal{R}_n^q$ rather than for the coefficients A_m^q. Then we combine the equations resulting from the projections of the boundary conditions in such a way to obtain $\mathbf{M}^q\mathcal{R}^q=V^q$. The matrix and the independent vector elements for s and p polarizations are given in Appendix D.

B. Infinite grating

Due to the pseudoperiodicity condition, the solution of the infinite grating problem is reduced to the solution of the problem in a single period (d) of the grating only, in which we have a bottle-shaped cavity. The space is divided into the same three regions described in Fig. 1. In regions 1 and 2 we keep the same expressions of the field inside the cavity used in Sec. II [Eq. (1)], but in region 3 we express the total field as the sum of the incident plane wave plus the field diffracted in the directions given by the grating equation,

$$f_3^q(x,y)=e^{i(\alpha_0x-\beta_0y)}+\sum_{n=-\infty}^{\infty}R_n^qe^{i(\alpha_nx+\beta_ny)}, \tag{14}$$

where α_0 and β_0 are defined in Sec. III A,

$$\alpha_n=k\sin\theta_n=\alpha_0+n\frac{2\pi}{d} \tag{15}$$

and

$$\beta_n=k\cos\theta_n=\sqrt{k^2-\alpha_n^2}. \tag{16}$$

Now we proceed as in the finite grating problem, but using Eq. (14) instead of Eq. (11). In the infinite grating case we are interested in calculating the efficiencies of the diffraction orders, which are given by

$$e_n=|R_n^q|^2\beta_n/\beta_0, \tag{17}$$

so we derive a matrix equation for the Rayleigh amplitudes R_n^q. Combining the equations that result from appropriate projections of the boundary conditions, we obtain a matrix equation $\mathbf{M}^qR^q=V^q$. The matrix and the independent vector elements for both polarizations are given in Appendix E.

IV. RESULTS AND DISCUSSION

As stated above, the purpose of this paper is to study the resonant behavior of bottle-shaped cavities, and its influence in the scattering patterns produced by a surface with one, N, or infinite identical cavities. In a previous paper we provided numerical evidence of a resonant enhancement of the field within a groove of this shape [9]. We found that for a surface with one groove, the curves of intensity scattered in the specular direction vs wavelength exhibit dips at certain wavelengths for both polarization modes. These wavelengths were associated with the resonant wavelengths of the cavity, since a strong enhacement of the field within the groove was found at those wavelengths. In addition, the calculated values are in agreement with the limit case of a rectangular waveguide. However, no independent calculation had been done for this particular profile to prove that these wavelengths correspond to surface shape resonances, i.e., to resonances associated with a local perturbation on an otherwise planar surface.

In Sec. IV A we give some numerical examples that show the surface shape resonant modes in the structure of Fig. 1, for both polarizations. Then, in Sec. IV B we show that those modes become apparent in the far field scattered from finite and infinite gratings made of identical cavities.

A. Eigenmodes of the cavity

As explained in Sec. II, to find the resonant wavelengths of an open cavity implies finding the zeros of the equation $\det[\mathbf{M}^q]=0$. However, instead of dealing with the sometimes difficult task of finding the complex roots of a complex determinant, another way of locating the resonant parameters—already used for other profiles of the surface in Refs. [14,15,7] is used here. It consists in evaluating numerically the function $|\det[\mathbf{M}^q(\lambda,h)]|^{-2}$, and the plot of this function versus the real part of the resonant wavelength (or the resonant depth) consists of a series of Lorentzian peaks of the form

$$|\det[\mathbf{M}^q(h)]|^{-2}\approx\frac{B}{[(h-h_R)^2+h_I^2]}, \tag{18}$$

where $h=h_R+ih_I$ is the complex root of $\det[\mathbf{M}^q(h)]$.

In Figs. 2–5 we plot $|\det[\mathbf{M}^q]|^{-2}$ versus the depth h_1 of the cavity, for a fixed wavelength. To check the validity of the results we first considered the case of a cavity with a

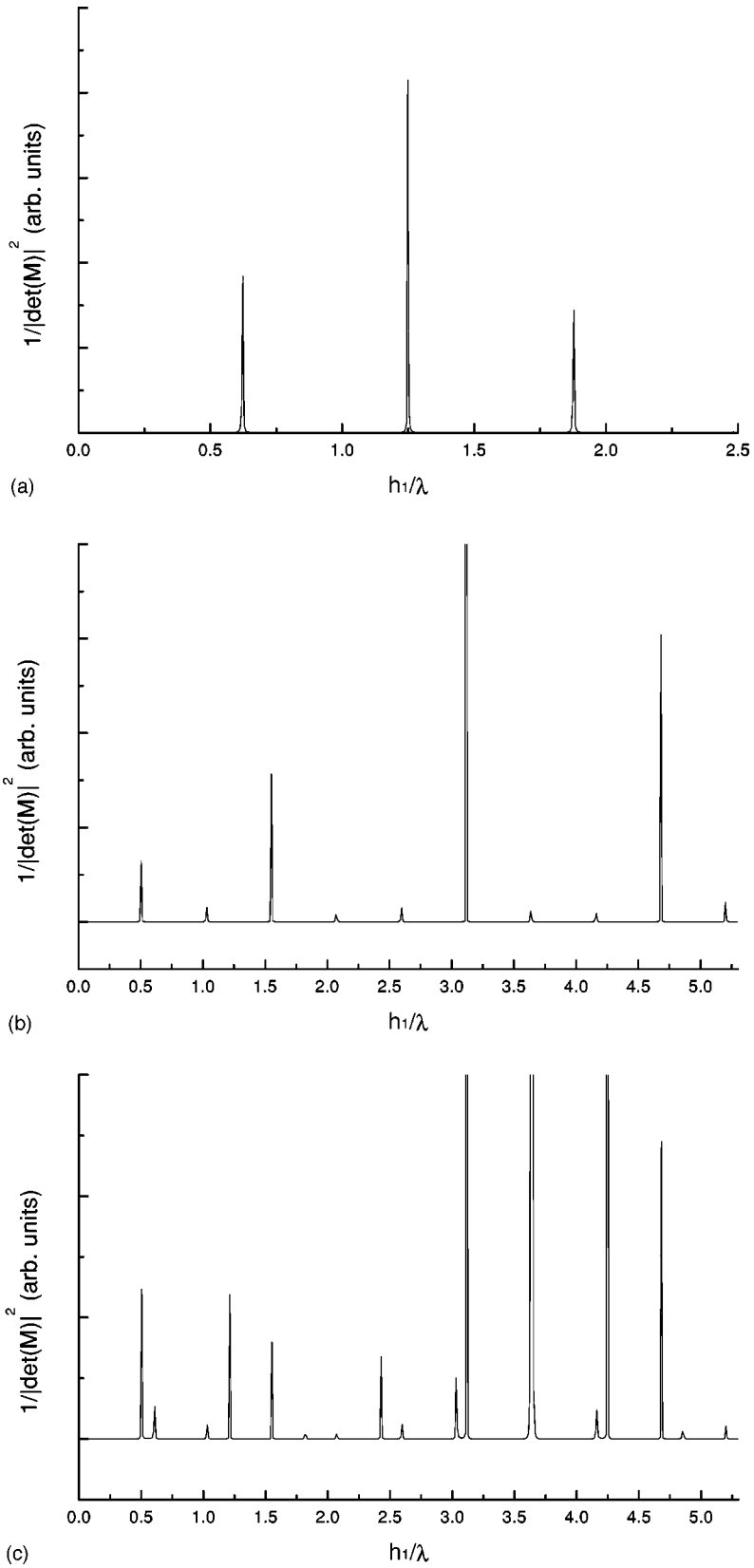

FIG. 2. $|\det(M^s)|^{-2}$ as a function of the depth h_1/λ for a bottle-shaped cavity of $h_1=0.9h$ and s polarization: (a) $c_1=0.828\lambda$ and $c_2=0.092\lambda$, (b) $c_1=1.764\lambda$ and $c_2=0.196\lambda$ $(m=1)$, and (c) $c_1=1.764\lambda$ and $c_2=0.196\lambda$ $(m=2)$.

narrow neck, so as to simulate the limit case of a rectangular waveguide of depth h_1 (Figs. 2 and 3). Figure 2 corresponds to s polarization, and Fig. 3 to p polarization. In Fig. 2(a), corresponding to a cavity with $c_1=0.828\lambda$, $c_2=0.092\lambda$, and $h=10h_1/9$, we observe three well-defined peaks in the range of h_1 considered. These peaks are located very close to the resonant depths of a rectangular waveguide, which are given by

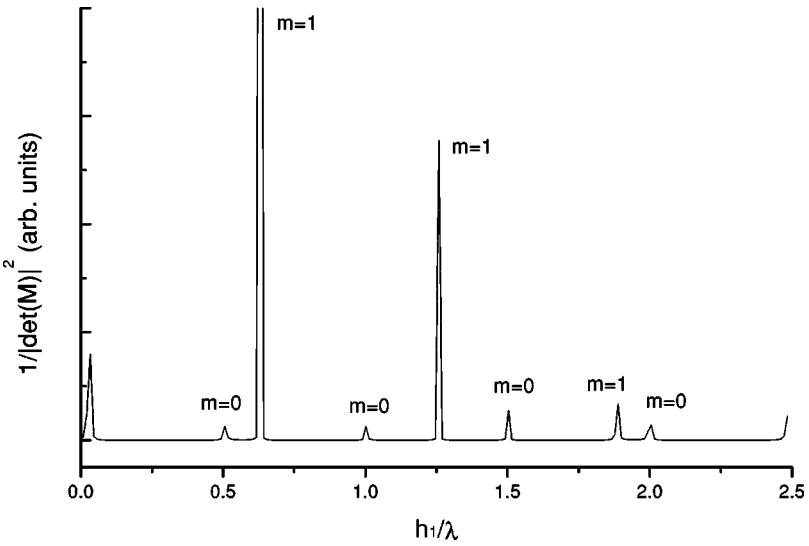

FIG. 3. $|\det(M^p)|^{-2}$ as a function of the depth h_1/λ for a bottle-shaped cavity of $h_1=0.9h$ and p polarization. $c_1=0.828\lambda$ and $c_2=0.092\lambda$.

$$\frac{h_1}{\lambda}=\frac{n}{\sqrt{4-\left(\frac{m\lambda}{c_1}\right)^2}}, \tag{19}$$

whose first three real values (corresponding to $m=1$) are $h_1/\lambda=0.625$, 1.254, and 1.876. We considered only eigenmodes with $m=1$, since the geometry of this cavity is such that there is only one real value of μ_m (which corresponds to $m=1$) and the other values of μ_m (with $m>1$) are purely imaginary. Then, the main contribution to the field inside the cavity comes from the first mode in the modal representation (1). Consequently, the curves obtained using only the first mode or using several modes have exactly the same peaks, as expected. In the case considered in Figs. 2(b) and 2(c), the wavelength was decreased so as to have two real values of μ_m, and then the parameters of the groove are $c_1=1.764\lambda$, $c_2=0.196\lambda$, and $h=10h_1/9$. If we only keep the first mode in the modal expansion, we obtain the curve in Fig. 2(b), which exhibits peaks associated with the resonant values of h_1 corresponding to $m=1$ in Eq. (19). However, if we keep two or more modes in the representation, we obtain the curve in Fig. 2(c), which in addition to the peaks in Fig. 2(b) has new peaks corresponding to resonant depths of the second mode. The resonant values of h_1 corresponding to the rectangular waveguide of these parameters were calculated using Eq. (19), and are listed in Table I. It can be noted from a comparison of Table I with the plot in Fig. 2(c) that the positions of the peaks agree very well with the predicted limit values. For p polarization (Fig. 3) we consider a cavity with the same parameters as those in Fig. 2(a). However, since the term with $m=0$ in Eq. (1) gives a nonzero contribution to the field inside the cavity, and it is in fact the fundamental mode of the cavity, in the p case there are two real values of μ_m. Hence we must consider at least the first two terms in the modal expansion to perform the curve in Fig. 3, where it is easy to associate the peaks with the dif-

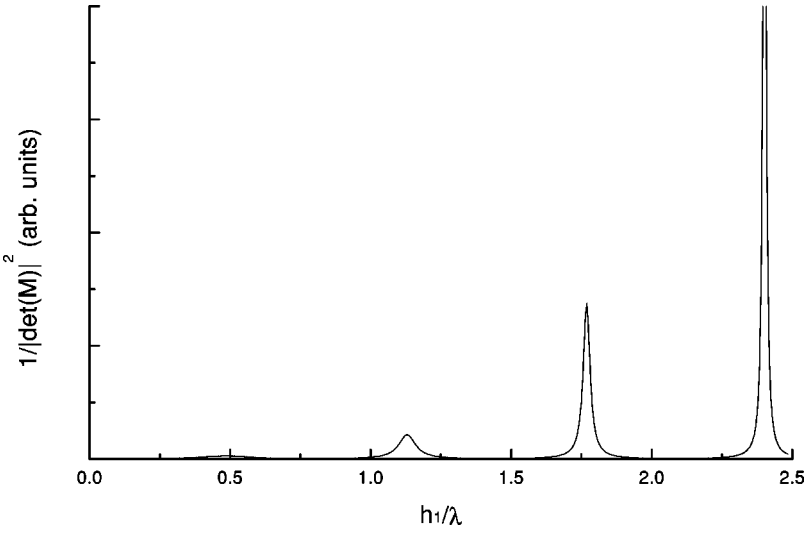

FIG. 4. $|\det(M^s)|^{-2}$ as a function of the depth h_1/λ for a bottle-shaped cavity of $h_1=0.9h$ and s polarization. $c_1=0.828\lambda$ and $c_2=0.368\lambda$.

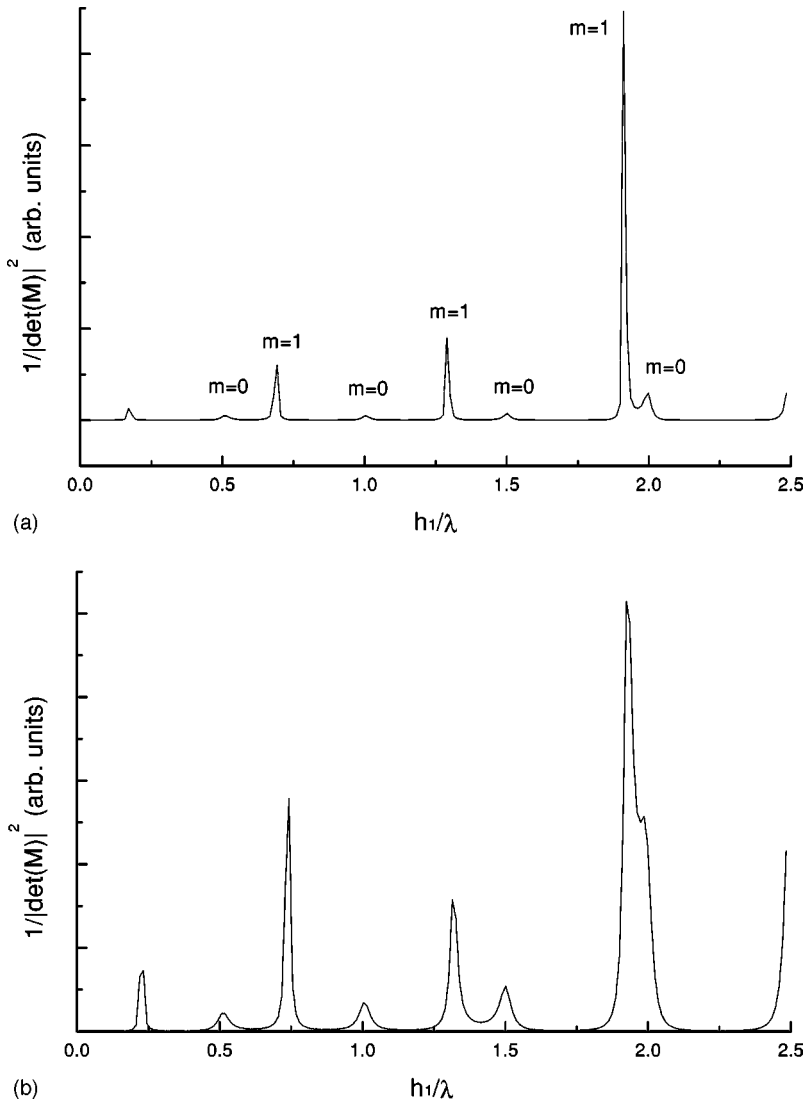

FIG. 5. $|\det(M^p)|^{-2}$ as a function of the depth h_1/λ for a bottle-shaped cavity of $h_1=0.9h$ and p polarization: (a) $c_1=0.828\lambda$ and $c_2=0.368\lambda$, and (b) $c_1=0.828\lambda$ and $c_2=0.552\lambda$.

ferent resonant values corresponding to $m=0$ and 1, by comparing their positions with the limit values listed in Table II.

In Fig. 4 we consider a cavity with a wider neck, $c_1=0.828\lambda$ and $c_2=0.368\lambda$, for s polarization. It can be noticed that now the peaks are wider than those in Fig. 2(a), indicating that the quality factors of these resonances are smaller. The same cavity but in the p case is considered in Fig. 5(a), where the peaks corresponding to the modes with $m=0$ and 1 are identified. These peaks are also wider than those in Fig. 3, and for a cavity with $c_2=0.552\lambda$ the peaks become even wider [see Fig. 5(b)]. The positions of the peaks also change if the width c_2 is changed, and sometimes two peaks can merge one into the other, forming only one peak, as can be observed in Fig. 5(b), near $h_1/\lambda\approx 1.9$.

TABLE I. Resonant values of the depth h/λ for a rectangular waveguide of width $c/\lambda=1.764$ in s polarization.

$n\|m$	1	2
1	0.519	0.605
2	1.041	1.211
3	1.562	1.819
4	2.084	2.425
5	2.605	3.033
6	3.127	3.639
7	3.649	4.247
8	4.170	4.852
9	4.692	5.460
10	5.196	6.066

TABLE II. Resonant values of the depth h/λ for a rectangular waveguide of width $c/\lambda=0.828$ in p polarization.

$n\|m$	0	1
1	0.5	0.627
2	1.0	1.254
3	1.5	1.881
4	2.0	2.509
5	2.5	3.136

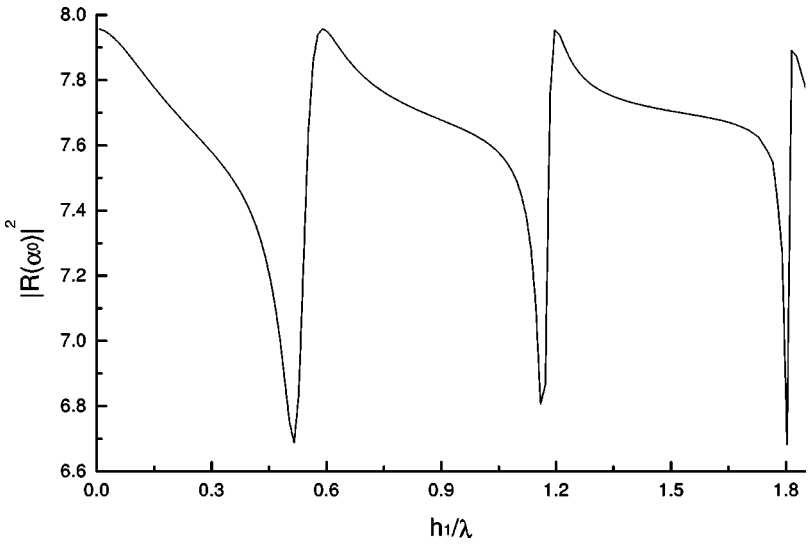

FIG. 6. Intensity scattered in the specular direction ($|\mathcal{R}^s(\alpha_0)|^2$) as a function of the depth h_1/λ, for a normally incident *s*-polarized Gaussian beam of width $w=9.2\lambda$ illuminating a surface with a single groove of $c_1=0.828\lambda$, $c_2=0.368\lambda$, and $h_1=0.9h$.

B. Scattering from finite and infinite gratings

In the following figures we illustrate the effects produced by the surface shape resonances in the scattering pattern from finite and infinite gratings. In Fig. 6 we consider an *s*-polarized Gaussian beam of width $w=9.2\lambda$ normally incident on a surface with a single cavity of $c_1=0.828\lambda$, $c_2=0.368\lambda$, and $h_1=0.9h$. The plot of specularly reflected intensity versus h_1/λ exhibits three dips at positions very close to those corresponding to the peaks in Fig. 4. This fact suggests that in resonant conditions the power scattered out of the specular direction increases. For the parameters chosen in this example, the main contribution to the field inside the cavity comes from the first mode, which is an even mode, and then the effects of the resonant behavior of the surface can be observed for normal incidence, i.e., for a symmetric configuration. If the number of cavities in the surface is increased, the dips become more pronounced but stay at the same positions (not shown). The *p* case is considered in Fig. 7, where we plot the specularly reflected intensity versus h_1/λ for a surface with cavities of the same parameters as those in Fig. 6. We consider the particular case where all the cavities are identical and equally spaced, the distance between their centers being $d=0.92\lambda$. Comparing Figs. 7(a) and 5(a), it can be noted that the position of the dips coincide with the peaks identified with the $m=0$ mode in Fig. 5(a). As stated above, an increase in the number of grooves makes the dips deeper, but the position is not altered. Since the normal illumination imposes the symmetry on the fields, only the even modes are excited in this situation. However, the second mode (which is an odd mode) also contributes significantly to the field inside the cavity, but its effects in the reflected intensity can only be appreciated by means of an oblique illumination. In Fig. 7(b) we plot the intensity reflected in the specular direction for a beam impinging upon the surface with an angle $\theta_0=45°$. In this case, not only the dips corresponding to the even modes but also the resonances associated with the mode $m=1$ appear as sharp and well-defined dips, located at the positions of the peaks in Fig. 5(a). These resonances seem to be more sensitive to a small change in h_1, and have better quality.

From the comparison of Figs. 6 and 7 with Figs. 4 and 5, we conclude that the occurrence of dips in the field intensity specularly reflected from finite gratings made of bottle-shaped grooves is intimately connected with the excitation of surface shape resonances inside the cavities. This result and a similar result obtained for cavities with circular cross section [16], suggest that this effect appears whenever the profile of the groove is double valued. In such cases, at certain wavelengths the electromagnetic field couples to the eigenmodes of the cavity and produces a spreading out of the reflected power. The existence of dips in the intensity reflected in the specular direction (in the examples presented this direction coincides with the normal direction) at the surface shape resonances of the structure is consistent with the results and discussion in Ref. [7]. In that paper the authors show that the differential reflection coefficient (DRC) *for scattering angles far from the specular* exhibit dips at certain wavelengths at which the perfect conductor boundary conditions are almost restored at the top of the surface. These minima should not be attributed to the excitation of surface shape resonances. However, it was shown in Fig. 3 of Ref. [7] that for scattering angles close to the specular direction the dips found in the DRC are associated with surface shape resonances, as predicted by the results of the homogeneous problem.

The last set of figures illustrates the effects produced by the resonant behavior of the cavities in the efficiency distribution of an infinite grating made of bottle-shaped grooves. In Fig. 8(a) we consider an infinite grating of $c_1/d=0.9$, $c_2/d=0.4$, $\lambda/d=1.0871$, and $h_1=0.9h$, where d is the grating period, illuminated by an *s*-polarized plane wave incident with an angle $\theta_0=45°$. It can be noted that the efficiency of the zero order has minima (and the efficiency of the -1 order has maxima) at the depths predicted by the peaks in Fig. 4. Even though the power conservation law imposes that the sum of the reflected efficiencies be 1, the distribution of energy among the diffraction orders (in this case only the 0 and -1 are propagating orders) reveals a strong dependence on the surface shape resonances. The behavior of the infinite grating is in agreement with that observed for a surface with a single groove and normal incidence (Fig. 6), which shows

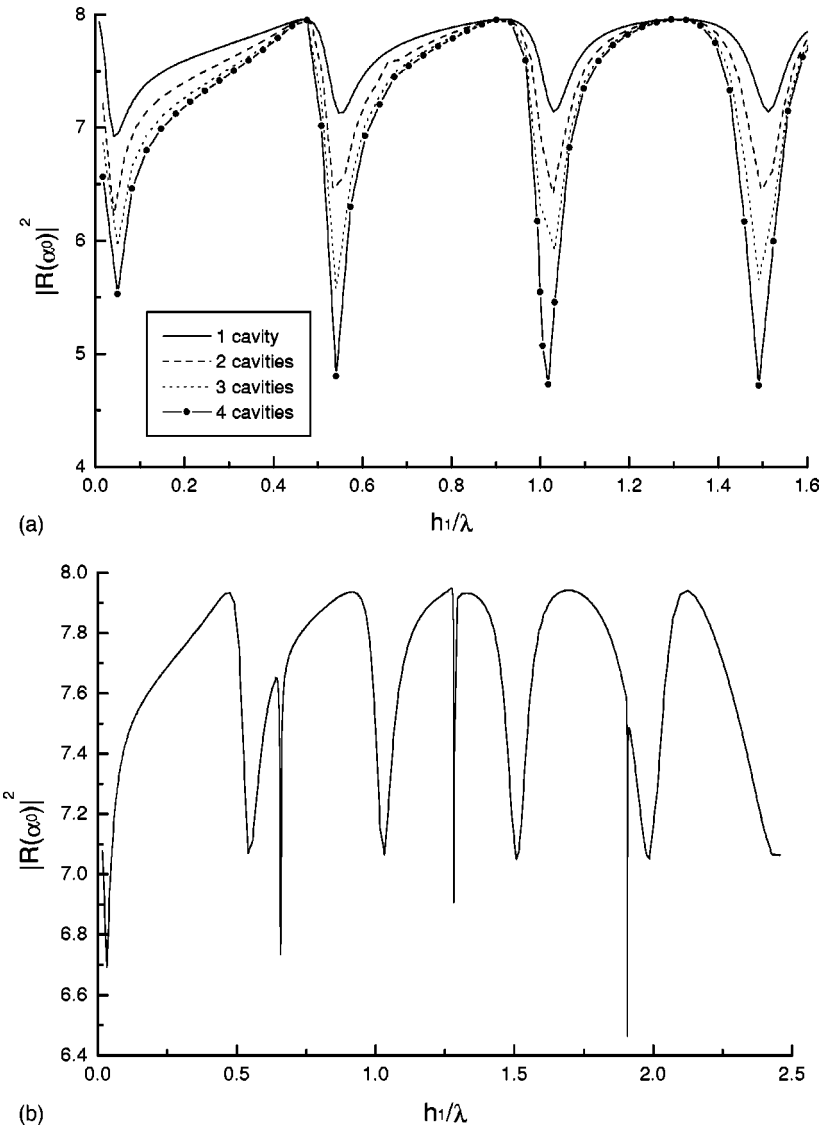

FIG. 7. Intensity scattered in the specular direction ($|\mathcal{R}^p(\alpha_0)|^2$) as a function of the depth h_1/λ, for an incident *p*-polarized Gaussian beam of width $w=9.2\lambda$ illuminating different surfaces with one, two, three, and four cavities of $c_1=0.828\lambda$, $c_2=0.368\lambda$, and $h_1=0.9h$, separated a distance $d=0.92\lambda$: (a) $\theta_0=0°$, and (b) $\theta_0=45°$ (for a surface with a single cavity).

that the resonant depths do not depend on the angle of incidence, as expected. In Fig. 8(b), which corresponds to a grating with the same parameters as in Fig. 8(a) but with a narrower mouse of the cavities ($c_2/d=0.1$), the effect of a resonant depth is clearly present in the 0 order efficiency curve at $h_1/d=0.68$, where the curve in Fig. 2(a) has a peak. Since this resonance has a higher quality than those in Fig. 8(a), the effect in the efficiency curve is more localized. In Fig. 9 we show efficiency curves for the same grating of Fig. 8(a) but under *p*-polarized illumination. According to what was observed for the finite grating [Fig. 7(b)], the efficiency reflected in the specular direction (order 0) has minima at the resonant depths [Fig. 9(a)]. These minima are zeros for the resonances corresponding to $m=0$, showing that for these resonant depths there is no energy reflected in the specular direction and all the power goes into the only other direction allowed: the -1 order. However, the $m=1$ resonances appear as sharper peaks revealing a more sensitive phenomenon [see Fig. 9(b)]. The minima in the zero order efficiency curve are compensated for by maxima in the -1 order efficiency curve, as required by the perfect conductor boundary conditions.

The results in Figs. 8 and 9 confirm that the distribution of reflected power is significantly modified at the resonant wavelengths of the cavity, even for infinite gratings. The anomalies in the reflected efficiency could be used to detect surface shape resonances in the far field.

V. CONCLUSION

In this paper we have calculated the surface shape resonances associated with a bottle-shaped cavity on a perfectly conducting plane for both *s* and *p* polarizations. We used a modal approach to solve the homogeneous problem as well as to solve the scattering problem from finite and infinite gratings. We found the resonant wavelengths (or depths) of the cavity by numerically evaluating the determinant of the scattering matrix. We checked the resonant depths by comparing them in the limit case of a rectangular waveguide, and obtained a very good agreement between them. It was shown

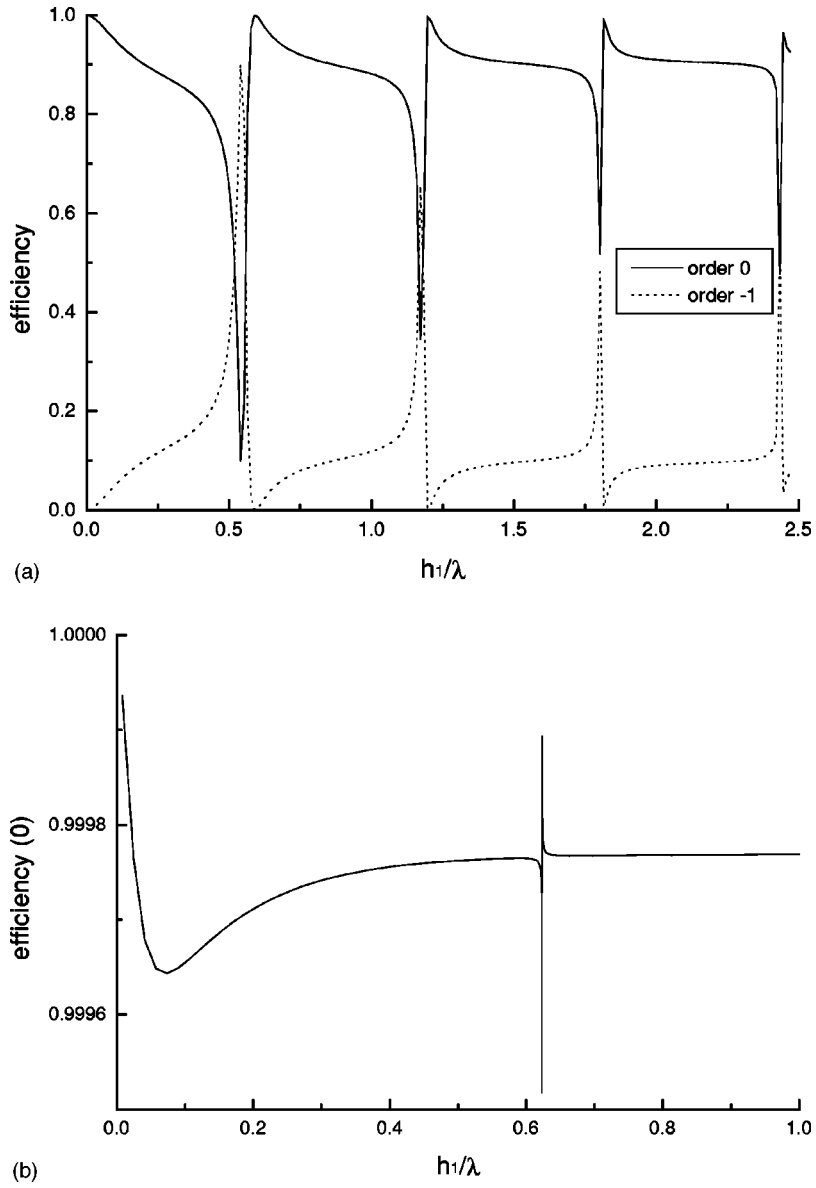

FIG. 8. Efficiency of the zero and -1 diffraction orders as a function of the depth h_1/d, from an infinite grating with a bottle-shaped cavity in a period. $c_1=0.9d$, $\lambda=1.087155743d$, $h_1=0.9h$, $\theta_0=45°$, and s polarization. (a) $c_2=0.4d$. (b) $c_2=0.1d$.

that the intensity scattered from a finite grating exhibits dips at the resonant depths of the cavity. Examples revealing the excitation of even and odd modes have been addressed. We also investigated the influence of the resonant excitation on the efficiencies of an infinitely periodic grating, and found that at the resonant depths the distribution of efficiencies is significantly modified. The examples presented in this paper exhibit polarization dependent features that could be attractive in several applications such as filters and polarizers. From a theoretical point of view, this study also constitutes a first step in the investigation of the possibility of exciting *s*-polarized surface waves in metallic infinite gratings, which will be the subject of future research.

ACKNOWLEDGMENTS

This work was supported by the Agencia para la Promoción Científica y Tecnológica under Grant No. BID802/OC-AR-PICT03-04457 and by the Universidad de Buenos Aires.

APPENDIX A: PROJECTED EQUATIONS FOR BOTH POLARIZATIONS

s polarization

$$A_m^s \sin(\mu_{m1}h_1)\frac{c_1}{2}=\sum_{n=1}^{\infty} I_{nm}^s[-a_n^s \sin(\mu_{n2}h_2) + b_n^s \cos(\mu_{n2}h_2)], \tag{A1}$$

$$\sum_{n=1}^{\infty} A_n^s \mu_{n1}\cos(\mu_{n1}h_1)I_{mn}^s=\frac{c_2}{2}\mu_{m2}[a_m^s \cos(\mu_{m2}h_2) + b_m^s \sin(\mu_{m2}h_2)], \tag{A2}$$

$$2\pi\mathcal{R}(\alpha)=\sum_{n=1}^{\infty} b_n^s J_n^s(-\alpha), \tag{A3}$$

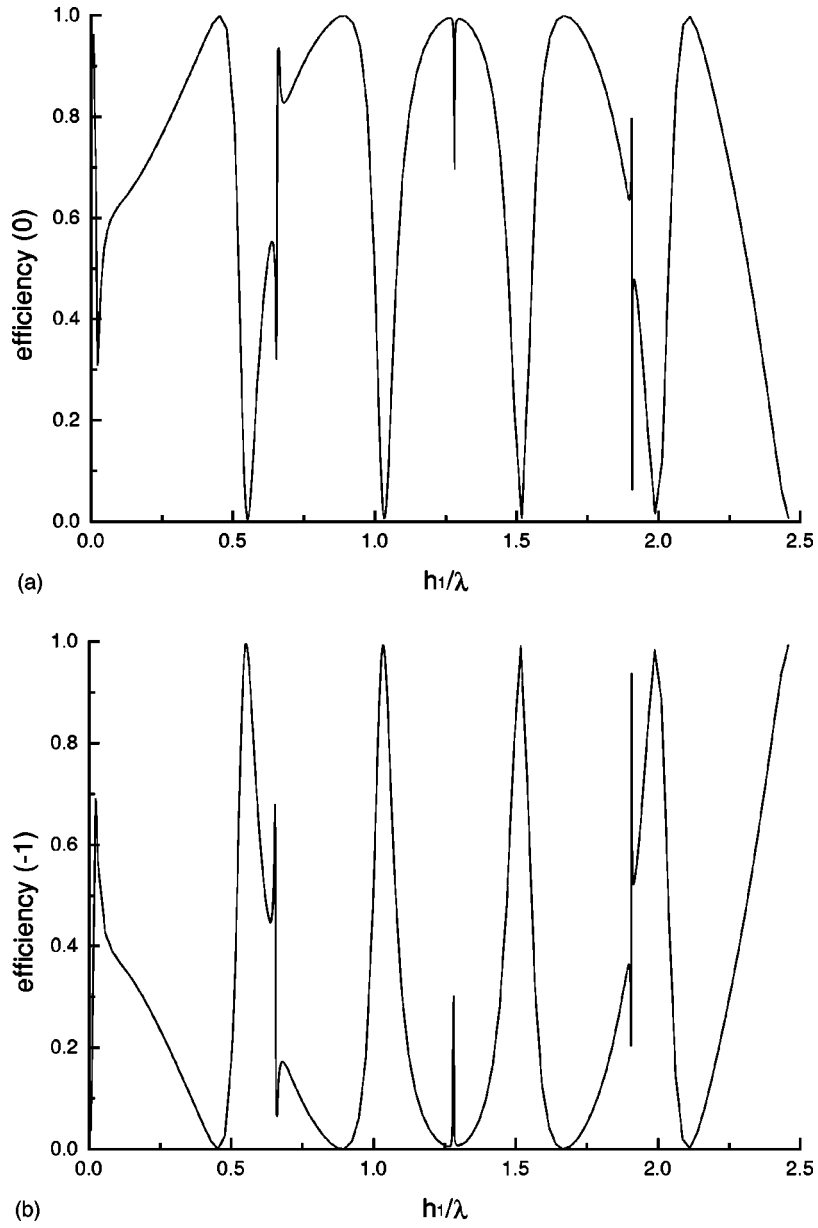

FIG. 9. Efficiency of the diffraction orders as a function of the depth h_1/d, from an infinite grating with a bottle-shaped cavity in a period. $c_1=0.9d$, $c_2=0.4d$, $\lambda=1.087155743d$, $h_1=0.9h$, $\theta_0=45°$, and p polarization. (a) order 0. (b) order -1.

$$i\int_{-\infty}^{\infty}\beta\mathcal{R}(\alpha)J_m^s(\alpha)d\alpha=\mu_{m2}a_m^s\frac{c_2}{2}, \tag{A4}$$

where

$$I_{nm}^s=\int_0^{c_2}\sin\left[\frac{n\pi x}{c_2}\right]\sin\left[\frac{m\pi}{c_1}(x-x_1)\right]dx \tag{A5}$$

and

$$J_n^s(\alpha)=\int_0^{c_2}\sin\left[\frac{n\pi x}{c_2}\right]\exp(i\alpha x)dx. \tag{A6}$$

p polarization

$$-A_m^p\sin(\mu_{m1}h_1)\mu_{m1}c_{1m}=\sum_{n=0}^{\infty}I_{nm}^p\mu_{n2}[a_n^p\cos(\mu_{n2}h_2)+b_n^p\sin(\mu_{n2}h_2)], \tag{A7}$$

$$\sum_{n=0}^{\infty}A_n^p\cos(\mu_{n1}h_1)I_{mn}^p=c_{2m}[-a_m^p\sin(\mu_{m2}h_2)+b_m^p\cos(\mu_{m2}h_2)], \tag{A8}$$

$$2\pi i\beta\mathcal{R}(\alpha)=\sum_{n=0}^{\infty}a_n^p\mu_{n2}J_n^p(-\alpha), \tag{A9}$$

$$\int_{-\infty}^{\infty}\mathcal{R}(\alpha)J_m^p(\alpha)d\alpha=b_m^pc_{2m}, \tag{A10}$$

where

$$I_{nm}^{p}=\int_{0}^{c_2}\cos\left[\frac{n\pi x}{c_2}\right]\cos\left[\frac{m\pi}{c_1}(x-x_1)\right]dx, \tag{A11}$$

$$J_{n}^{p}(\alpha)=\int_{0}^{c_2}\cos\left[\frac{n\pi x}{c_2}\right]\exp(i\alpha x)dx, \tag{A12}$$

and

$$c_{jm}=\begin{cases} c_j & \text{if } m=0 \\ c_j/2 & \text{if } m\neq 0 \end{cases} \quad j=1,2. \tag{A13}$$

APPENDIX B: EXPLICIT EXPRESSIONS OF THE MATRIX ELEMENTS IN EQ. (9)

s polarization

$$\mathbf{M}_{mn}^{s}=\mu_{n1}\cos(\mu_{n1}h_1)\sum_{j=1}^{\infty}I_{jn}^{s}\sum_{k=1}^{\infty}(\mathbf{B}^{s})_{kj}^{-1}\sum_{q=1}^{\infty}\mathbf{C}_{qk}^{s}I_{qm}^{s}-\frac{c_1}{2}\sin(\mu_{m1}h_1)\delta_{mn}, \tag{B1}$$

where

$$\mathbf{B}_{kj}^{s}=\mu_{k2}\frac{c_2}{2}[\mathbf{A}_{kj}^{s}\cos(\mu_{k2}h_2)+\sin(\mu_{k2}h_2)\delta_{kj}], \tag{B2}$$

$$\mathbf{C}_{kj}^{s}=-\mathbf{A}_{kj}^{s}\sin(\mu_{k2}h_2)+\cos(\mu_{k2}h_2)\delta_{kj}, \tag{B3}$$

and

$$\mathbf{A}_{kj}^{s}=\frac{i}{\pi}\frac{1}{\mu_{k2}c_2}\int_{-\infty}^{\infty}\beta J_{k}^{s}(\alpha)J_{j}^{s}(-\alpha)d\alpha. \tag{B4}$$

p polarization

$$\mathbf{M}_{mn}^{p}=\cos(\mu_{n1}h_1)\sum_{j=0}^{\infty}I_{jn}^{p}\sum_{k=0}^{\infty}(\mathbf{B}^{p})_{kj}^{-1}\sum_{q=0}^{\infty}\mu_{q2}I_{qm}^{p}\mathbf{C}_{qk}^{p}+\mu_{m1}c_{1m}\sin(\mu_{m1}h_1)\delta_{mn}, \tag{B5}$$

$$\mathbf{B}_{kj}^{p}=c_{2k}[\mathbf{A}_{kj}^{p}\cos(\mu_{k2}h_2)-\sin(\mu_{k2}h_2)\delta_{kj}], \tag{B6}$$

$$\mathbf{C}_{kj}^{p}=\mathbf{A}_{kj}^{p}\sin(\mu_{k2}h_2)+\cos(\mu_{k2}h_2)\delta_{kj}, \tag{B7}$$

and

$$\mathbf{A}_{kj}^{p}=\frac{\mu_{j2}}{2\pi i c_{2k}}\int_{-\infty}^{\infty}\frac{1}{\beta}J_{k}^{p}(\alpha)J_{j}^{p}(-\alpha)d\alpha. \tag{B8}$$

APPENDIX C: MODAL FUNCTIONS IN REGIONS 1 AND 2

$$u_{1m}^{ql}(x)=\begin{cases}\sin\left[\dfrac{m\pi}{c_1^{l}}(x-x_1^{l})\right] & \text{for } q=s \\ \cos\left[\dfrac{m\pi}{c_1^{l}}(x-x_1^{l})\right] & \text{for } q=p,\end{cases} \tag{C1}$$

$$w_{1m}^{ql}(y)=\begin{cases}A_m^{sl}\sin[\mu_{m1}^{l}(y+h)] & \text{for } q=s \\ A_m^{pl}\cos[\mu_{m1}^{l}(y+h)] & \text{for } q=p,\end{cases} \tag{C2}$$

$$u_{2m}^{ql}(x)=\begin{cases}\sin\left[\dfrac{m\pi}{c_2^{l}}(x-x_2^{l})\right] & \text{for } q=s \\ \cos\left[\dfrac{m\pi}{c_2^{l}}(x-x_2^{l})\right] & \text{for } q=p,\end{cases} \tag{C3}$$

$$w_{2m}^{ql}(y)=[a_m^{ql}\sin(\mu_{m2}^{l}y)+b_m^{ql}\cos(\mu_{m2}^{l}y)], \quad q=s,p, \tag{C4}$$

$$\mu_{mj}^{l}=\begin{cases}\sqrt{k^2-\left[\dfrac{m\pi}{c_j^{l}}\right]^2} & \text{if } k^2>\left[\dfrac{m\pi}{c_j^{l}}\right]^2 \\ i\sqrt{\left[\dfrac{m\pi}{c_j^{l}}\right]^2-k^2} & \text{if } k^2<\left[\dfrac{m\pi}{c_j^{l}}\right]^2,\end{cases} \tag{C5}$$

$$\mathrm{rect}(s)=\begin{cases}1 & 0<s<1 \\ 0 & \text{otherwise.}\end{cases} \tag{C6}$$

A_m^{ql}, a_m^{ql}, and b_m^{ql} are the unknown modal amplitudes, the superscript l denotes the groove, and x_1^{l} and x_2^{l} are the starting x coordinates of the lower and upper parts of the lth groove, respectively.

APPENDIX D: MATRIX AND INDEPENDENT VECTOR ELEMENTS FOR THE FINITE GRATING PROBLEM

$$\mathbf{M}_{mn}^{s}=i\Delta\alpha\beta_n\sum_{l=1}^{N}\frac{e^{i(\alpha_n-\alpha_m)x_2^{l}}}{c_2^{l}}\sum_{k=1}^{\infty}\sum_{j=1}^{\infty}\frac{1}{\mu_{k2}^{l}}J_j^{sl}(\alpha_m)^{*}J_k^{sl}(\alpha_n)\times[(P^{sl})^{-1}Q^{sl}]_{jk}-\pi\delta_{mn}, \tag{D1}$$

$$V_m^{s}=i\Delta\alpha\sum_{n=1}^{\infty}\beta_n\mathcal{A}_n\sum_{l=1}^{N}\frac{e^{i(\alpha_n-\alpha_m)x_2^{l}}}{c_2^{l}}\times\sum_{k=1}^{\infty}\sum_{j=1}^{\infty}\frac{1}{\mu_{k2}^{l}}J_j^{sl}(\alpha_m)^{*}J_k^{sl}(\alpha_n)[(P^{sl})^{-1}Q^{sl})]_{jk}+\pi\mathcal{A}_m, \tag{D2}$$

$$\mathbf{M}_{mn}^{p}=-\Delta\alpha\sum_{l=1}^{N}e^{i(\alpha_n-\alpha_m)x_2^{l}}\sum_{k=0}^{\infty}\sum_{j=0}^{\infty}\frac{\mu_{j2}^{l}}{c_{2k}^{l}}J_j^{pl}(\alpha_m)^{*}J_k^{pl}(\alpha_n)\times[(P^{pl})^{-1}Q^{pl}]_{jk}+2\pi i\beta_m\delta_{mn}, \tag{D3}$$

$$V_m^p=\Delta\alpha\sum_{n=1}^{\infty}\mathcal{A}_n\sum_{l=1}^{N}e^{i(\alpha_n-\alpha_m)x_2^l}\times\sum_{k=0}^{\infty}\sum_{j=0}^{\infty}\frac{\mu_{j2}^l}{c_{2k}^l}J_j^{pl}(\alpha_m)^*J_k^{pl}(\alpha_n)[(P^{pl})^{-1}Q^{pl}]_{jk}+2\pi i\beta_m\mathcal{A}_m, \tag{D4}$$

where $\mathcal{A}_m=\mathcal{A}(\alpha_m)$,

$$P_{jk}^{sl}=\sum_{m=1}^{\infty}\frac{4\mu_{m1}^l\cot(\mu_{m1}^lh_1)\cos(\mu_{k2}^lh_2)}{c_1^lc_2^l\mu_{j2}^l\cos(\mu_{j2}^lh_2)}\mathbf{D}_{mj}^{sl}\mathbf{D}_{mk}^{sl}-\tan(\mu_{j2}^lh_2)\delta_{jk}, \tag{D5}$$

$$Q_{jk}^{sl}=\sum_{m=1}^{\infty}\frac{4\mu_{m1}^l\cot(\mu_{m1}^lh_1)\sin(\mu_{k2}^lh_2)}{c_1^lc_2^l\mu_{j2}^l\cos(\mu_{j2}^lh_2)}\mathbf{D}_{mj}^{sl}\mathbf{D}_{mk}^{sl}+\delta_{jk}, \tag{D6}$$

$$P_{jk}^{pl}=-\sum_{m=0}^{\infty}\frac{\mu_{k2}^l\cot(\mu_{j1}^lh_1)\cos(\mu_{k2}^lh_2)}{c_{1m}^lc_{2j}^l\mu_{m1}^l\cos(\mu_{j2}^lh_2)}\mathbf{D}_{mj}^{pl}\mathbf{D}_{mk}^{pl}+\tan(\mu_{j2}^lh_2)\delta_{jk}, \tag{D7}$$

$$Q_{jk}^{pl}=\sum_{m=0}^{\infty}\frac{\mu_{k2}^l\cot(\mu_{m1}^lh_1)\sin(\mu_{k2}^lh_2)}{c_{1m}^lc_{2j}^l\mu_{m1}^l\cos(\mu_{j2}^lh_2)}\mathbf{D}_{mj}^{pl}\mathbf{D}_{mk}^{pl}+\delta_{jk}. \tag{D8}$$

$$\mathbf{D}_{mj}^{sl}=\int_{x_2^l}^{x_2^l+c_2^l}\sin\left[\frac{j\pi}{c_2^l}(x-x_2^l)\right]\sin\left[\frac{m\pi}{c_1^l}(x-x_1^l)\right]dx, \tag{D9}$$

$$\mathbf{D}_{mj}^{pl}=\int_{x_2^l}^{x_2^l+c_2^l}\cos\left[\frac{j\pi}{c_2^l}(x-x_2^l)\right]\cos\left[\frac{m\pi}{c_1^l}(x-x_1^l)\right]dx, \tag{D10}$$

and $J_k^{ql}(\alpha_n)$ are defined in Eqs. (A6) and (A12) by substituting c_2 by c_2^l.

APPENDIX E: MATRIX AND INDEPENDENT VECTOR ELEMENTS FOR THE INFINITE GRATING PROBLEM

s polarization

$$\mathbf{M}_{mn}^s=\frac{2i}{c_2}\sum_{k=1}^{\infty}\sum_{j=1}^{\infty}\frac{\beta_n}{\mu_{k2}}J_j^s(\alpha_m)^*J_k^s(\alpha_n)(P^{(s)-1}Q^s)_{jk}-d\delta_{mn}, \tag{E1}$$

$$V_m^s=\frac{2i\beta_0}{c_2}\sum_{k=1}^{\infty}\sum_{j=1}^{\infty}\frac{1}{\mu_{k2}}J_j^s(\alpha_m)^*J_k^s(\alpha_0)(P^{(s)-1}Q^s)_{jk}+d\delta_{m0}. \tag{E2}$$

p polarization

$$\mathbf{M}_{mn}^p=\sum_{k=0}^{\infty}\sum_{j=0}^{\infty}\frac{\mu_{j2}}{c_2(k)}J_j^p(\alpha_m)^*J_k^p(\alpha_n)(P^{(p)-1}Q^p)_{jk}-i\beta_md\delta_{mn}, \tag{E3}$$

$$V_m^p=-\sum_{k=0}^{\infty}\sum_{j=0}^{\infty}\frac{\mu_{j2}}{c_2(k)}J_j^p(\alpha_m)^*J_k^p(\alpha_0)(P^{(p)-1}Q^p)_{jk}-i\beta_0d\delta_{m0}, \tag{E4}$$

where the matrices P^q and Q^q are given by Eqs. (D5), (D6), (D7), and (D8) by suppressing the superscript *l*.

[1] A.A. Maradudin, T. Michel, A. McGurn, and E.R. Mendez, Ann. Phys. (N.Y.) **203**, 255 (1990).
[2] A. Hessel and A.A. Oliner, Appl. Opt. **4,**, 1275 (1965).
[3] J.R. Andrewartha, J.R. Fox, and I.J. Wilson, Opt. Acta **26**, 69 (1977).
[4] A. Wirgin and A.A. Maradudin, Phys. Rev. B **31**, 5573 (1985).
[5] D.C. Skigin and R.A. Depine, Optik (Stuttgart) **94**, 114 (1993).
[6] R.W. Ziolkowski and J.B. Grant, IEEE Trans. Antennas Propag. **35**, 504 (1987).
[7] A.A. Maradudin, A.V. Shchegrov, and T.A. Leskova, Opt. Commun. **135**, 352 (1997).
[8] C.I. Valencia and R.A. Depine, Opt. Commun. **159**, 254 (1999).
[9] D.C. Skigin and R.A. Depine, Phys. Rev. E **59**, 3661 (1999).
[10] S. Jovicevic and S. Sesnic, J. Opt. Soc. Am. **62**, 865 (1972).
[11] J.R. Andrewartha, G.H. Derrick, and R.C. McPhedran, Opt. Acta **28**, 1177 (1981).
[12] J.R. Andrewartha, G.H. Derrick, and R.C. McPhedran, Opt. Acta **28**, 1501 (1981).
[13] L. Li, J. Opt. Soc. Am. A **10**, 2581 (1993).
[14] A.A. Maradudin, P. Ryan, and A.R. McGurn, Phys. Rev. B **38**, 3068 (1988).
[15] A.V. Shchegrov and A.A. Maradudin, Appl. Phys. Lett. **67**, 3090 (1995).
[16] R. A. Depine and C. I. Valencia, J. Phys. D **32**, 1114 (1999).